

A mathematical method for quantifying in-vivo mechanical behaviour of heel pad under dynamic load

Roozbeh Naemi^{(1)(*)}, Panagiotis E. Chatzistergos⁽¹⁾, Nachiappan Chockalingam⁽¹⁾

(1) Faculty of Health Sciences, Staffordshire University, Stoke-on-Trent, United Kingdom.

(*) Corresponding author, **tel.:** +44 1782 295879

e-mail: r.naemi@staffs.ac.uk

Keywords: Biomechanics, Plantar soft tissue, ultrasound indentation, visco-elastic, Stress-strain model

Word count (5450)

Abstract (200 words)

4 figures

2 tables

Abstract:

Mechanical behaviour of the heel pad, as a shock attenuating interface during a foot strike, determines the loading on the musculo-skeletal system during walking. The mathematical models that describe the force deformation relationship of the heel pad structure can determine the mechanical behaviour of heel pad under load. Hence, the purpose of this study was to propose a method of quantifying the heel pad stress-strain relationship using force-deformation data from an indentation test.

The energy input and energy returned were calculated by numerically integrating the area below the stress-strain curve during loading and unloading respectively. Elastic energy and energy absorbed were calculated as the sum of and the difference between energy input and energy return respectively. By fitting the energy function derived from a nonlinear visco-elastic model to the energy- strain data, the elastic and viscous model parameters were quantified.

The viscous and elastic exponent model parameters were significantly correlated to maximum strain, indicating the need to perform indentation tests at realistic maximum strains relevant to walking. The proposed method showed to be able to differentiate between the elastic and viscous components of the heel pad response to loading and to allow quantifying the corresponding stress-strain model parameters.

Introduction

Heel pad represents a natural cushioning interface between the calcaneal bone and the ground, with the capacity to attenuate the impact during a heel strike [1] [2]. The heel pad consists of a fatty tissue separated by the septa creating a compartmentalised structure [3]. As the mechanical properties of this interface determine the reaction force-deformation behaviour of the heel pad during ground contact, this properties affect the loading of the musculo-skeletal system [4] . Mathematical models have been used to describe the reaction force-deformation behaviour of the heel pad, and several mathematical models have been utilised to investigate the heel pad behaviour in-vitro, in-situ and in-vivo [1, 5–14].

A number of mathematical models were developed to described the nonlinear visco-elastic behaviour of soft tissue during in-vitro testing [15, 16], some of which represent the reaction force-deformation behaviour of the plantar fat pad in-vivo [8, 10, 13, 17–20]. Despite this, most of the proposed in-vivo models only assessed the stiffness of the plantar heel pad, and there are only a few that considered viscosity that affects the energy return ability of the soft tissue during a loading cycle.

Both the elasticity and viscosity component play an important role in determining the behaviour of the soft tissue under load. Viscosity contributes to dissipation of energy during loading/unloading cycle and a significantly different energy dissipation ratio –defined as the energy dissipated to the energy during loading- between the diabetic groups ($36 \% \pm 8.7\%$) and healthy adult groups ($27.9 \% \pm 6.2\%$) [13] can be attributed to a higher level of plantar soft tissue viscosity between the two groups.

One of the in-vivo models that was proposed by Gefen et al. [10] utilised a visco-elastic model resembling the mechanical behaviour of a Voight-Kelvin model, where the elasticity and viscosity components were represented using a linear spring and a nonlinear damper respectively. Despite the clear improvement as a result of considering viscosity as a separate component in the proposed model by Gefen et al. [10], their assumption of linear elasticity can be scrutinised as an oversimplification of the elastic behaviour of soft tissue.

Furthermore while studying the mechanical behaviour of the heel pad during walking can enhance the potential relevance of the results [10] [21] the repeatability and the accuracy of the measurements can be compromised by variations in the loading conditions imposed to the heel pad because of different heel strike patterns within and between individuals.

In an attempt to study the mechanical behaviour of the plantar soft tissues under controlled and repeatable loading conditions different ultrasound indentation techniques have been developed [17, 19, 20, 22–26]. Ultrasound indentation has been commonly employed for the direct measurements of heel pad stiffness, energy dissipation ratio or combined with finite element modelling for the inverse engineering of bulk material hyper-elasticity coefficients [22, 27, 28]. Despite these there has been a paucity of studies in which mathematical modelling was utilised to study and quantify both the viscous and elastic aspect of the soft tissues' behaviour.

While a number of nonlinear mathematical models represented the reaction force-deformation pattern of shod foot [11, 18, 29] , the model proposed by Scott and Winter [30] was proved to adequately represent the reaction force-deformation behaviour of plantar fat pad [31].

In this model both the elastic and viscous force components are a nonlinear function of deformation. This is an improvement over the other existing models in which either viscosity was not taken into account [23] or in which a linear function was used for elasticity component [10]. In fact during quasi-static tests, in which only the elasticity component of heel pad results in resistance to compression, a non-linear force-deformation trend with strain stiffening was observed. The power function proposed in [30] proved to be an appropriate nonlinear function that takes into account the effect of strain stiffening. A schematic presentation of this model is presented in Figure (1).

Figure 1 here

In spite of this, the nonlinear visco-elastic model has never been utilised to determine the force-deformation behaviour of the heel pad, and there is no set method to determine the subject-specific model parameters that can reveal the behaviour of the heel pad in each individual.

The purpose of this study is to propose a method of quantifying the reaction force-deformation behaviour of the heel pad under compression that takes into account the nonlinear visco-elastic behaviour of the soft tissue. Furthermore the secondary purpose of this study was to identify the effect of target stress and strain rate on the stress-strain model parameter to provide more insight into the complex behaviour of plantar soft tissue under load.

Method

Ethical approval was sought and granted from the University Ethics Committee which followed the principles outlined in the Declaration of Helsinki, Ethical principles for Medical Research Involving Human Subjects. A male participant (weight: 80 kg, Height: 1.84 m and BMI: 23.6) provided a full informed consent before partaking in the study. The participant did not have any pathology and foot pain prior to participating in this study and was under any medication.

An ultrasound indentation device [32] was utilised to perform indentation of plantar soft tissue at the apex of calcaneus (Figure 2). This device comprises an 18 MHz linear array ultrasound probe with a footprint-area of 3.8 cm² connected in series with a load cell (3kN, INSTRON). The load cell and the ultrasound probe were connected using a custom made probe holder which was capable of gripping ultrasound probes of different sizes and shapes. The instrumented probe was mounted on a rigid metallic frame that was equipped with a ball screw linear actuator and a hand wheel for the manual application of loading as well as with adjustable foot support that can rigidly fix the subject's foot (Figure 2). A complete anti-clockwise revolution of the hand wheel generated 5 mm of linear movement in forward direction. The imposed displacement rate was controlled with the help of a metronome.

Figure 2 here

When the instrumented probe was pressed against the plantar aspect of the heel the heel pad is compressed between the indenting device (i.e. ultrasound probe) and the calcaneus. The applied force is recorded using a load cell and the initial thickness and the deformation of the heel pad was measured

from the ultrasound images with the help of video analysis software (Kinovea open source project, www.kinovea.org).

Prior to the indentation tests the participant was asked to walk across an instrumented walkway (Matscan, Tekscan Inc, USA) during which plantar pressure were collected during 2 consecutive stance phases from each trial. Three trials were collected and plantar pressure was averaged over three trials. The average plantar pressure over the stance phase was measured over a rectangular region that represented the area of indentation at the calcaneal tuberosity, which reached 265 kPa. This value was used to calculate the maximum load during the indentation tests to ensure that the compressive forces are within the average range that the heel pad experienced during walking.

Five different loading sets resembling 5 different loading scenarios involving different target deformation rates and target maximum loads were realized. More specifically the subject's heel pad was loaded at three different rates as defined by three different shaft average revolution per minute of 40, 60, 80 RPM to maximum load of 70 N. Furthermore to determine the effect of maximum load at constant loading rate (60 RPM) target maximum loads of 30 and 100 N, were examined. These together with a retest at 60RPM, 70 N produced 6 different sets of indentation tests to maximum stress and strain rates.

The deformation data was sampled at 28 Hz and was synchronised to the force data gathered from load cell, which sampled the applied force at the same frequency. To minimise the effect of loading history, like the type and intensity of physical activity before the tests, the participant was asked to sit on the couch with his feet hanging for 5 minutes prior to start of the ultrasound indentation test. The indentation was performed over 10 load/unload cycles at constant target deformation rate. To ensure consistency of the stress-strain data between cycles, the first seven load cycles as pre-conditioning and the last three were recorded for assessment. The force deformation data was normalised to the contact area and the initial thickness taking into account the probe head area and the initial plantar heel pad thickness. For simplicity the normalised force is referred to as "stress" and the normalised deformation is referred to as "strain". The data was then imported to Matlab (Mathworks Inc., 2010) curve fitting toolbox, where

a 9th order polynomial ($f(\epsilon) = P_1.\epsilon^9 + P_2.\epsilon^8 + P_3.\epsilon^7 + P_4.\epsilon^6 + P_5.\epsilon^5 + P_6.\epsilon^4 + P_7.\epsilon^3 + P_8.\epsilon^2 + P_9.\epsilon + P_{10}$) was separately fitted to the 3 curves of stress-strain data during loading and unloading. The polynomial provided an appropriate fit to the data with the fit goodness parameters as follows: $R^2 = 0.993 \pm 0.001$, Sum of Squared Errors (SSE) = $(3.033 \pm 0.471) \times 10^{10}$, and Root Mean Squared Error (RMSE) = 4941 ± 7.071 with the polynomial parameters quantified at 95% certainty level.

Calculation of energy input, returned and absorbed

Energy input (E_i) up to the strain (ϵ_j) was calculated by numerically integrating the area below the stress-strain polynomial curve from 0 to ϵ_j using strain interval $\Delta\epsilon=0.01$ during loading according to equation (1):

$$E_i(\epsilon_j) = \sum_{\epsilon=0}^{\epsilon_j} \sigma_l(\epsilon_j) \cdot \Delta\epsilon \quad \text{Equation 1}$$

Energy input ($E_{i(\epsilon_j)}$) was calculated for strains from 0 to max strain (ϵ_{\max}) at 0.01 strain interval.

Energy return (E_r) up to the strain (ϵ_j) was calculated by numerically integrating the area below the stress-strain polynomial curve from 0 to ϵ_j using strain interval $\Delta\epsilon=0.01$ during unloading according to equation (2) :

$$E_r(\epsilon_j) = \sum_{\epsilon=0}^{\epsilon_j} \sigma_u(\epsilon_j) \cdot \Delta\epsilon \quad \text{Equation 2}$$

Energy return ($E_{r(\epsilon_j)}$) was calculated for strains from 0 to max strain (ϵ_{\max}) at 0.01 strain interval.

Energy absorbed (E_h) up to the strain (ϵ_j) was calculated by subtracting the energy return from energy input up to the strain (ϵ_j) according to equation 3.

$$E_h(\epsilon_j) = E_i(\epsilon_j) - E_r(\epsilon_j) \quad \text{Equation 3}$$

Energy absorbed ($E_{h(\epsilon_j)}$) was calculated for strains from 0 to target strain (ϵ_{\max}) at 0.01 strain interval.

Extracting the reaction model parameters

A model consisting of a nonlinear spring parallel to a nonlinear damper [30] was considered to represent the stress-strain relationship during loading :

$$\sigma_l(\varepsilon) = a \cdot \varepsilon^b + c \cdot \varepsilon^d \cdot \dot{\varepsilon} \quad \text{Equation 4}$$

Where ε represents strain, $\dot{\varepsilon}$ represents strain rate and $\sigma_l(\varepsilon)$ represents stress during loading. $a \cdot \varepsilon^b$ represents the elastic stress, and $c \cdot \varepsilon^d \cdot \dot{\varepsilon}$ represents viscous stress. a and c are the scaling factors and b and d represent the exponents respectively.

The energy input (E_i) was determined by integrating the area below the stress-strain curve during loading according to below:

$$E_i(\varepsilon) = \int (a \cdot \varepsilon^b + c \cdot \varepsilon^d \cdot \dot{\varepsilon}) \cdot d\varepsilon \quad \text{Equation 5}$$

Where deformation rate is constant during loading, energy input (E_i) can be rewritten as:

$$E_i(\varepsilon) = \frac{a}{b+1} \cdot \varepsilon^{b+1} + \frac{c}{d+1} \cdot \varepsilon^{d+1} \cdot \dot{\varepsilon} \quad \text{Equation 6}$$

For a low strain rate the stress-strain relationship can be written during unloading as follows.

$$\sigma_u(\varepsilon) = a \cdot \varepsilon^b - c \cdot \varepsilon^d \cdot \dot{\varepsilon} \quad \text{Equation 7}$$

Where ε represents strain, $\dot{\varepsilon}$ represents strain rate and $\sigma_u(\varepsilon)$ represents stress during unloading. The energy returned (E_r) was determined by integrating the area below the stress-strain curve during unloading.

Where deformation rate is constant during unloading, energy return (E_r) can be rewritten as:

$$E_r(\varepsilon) = \frac{a}{b+1} \cdot \varepsilon^{b+1} - \frac{c}{d+1} \cdot \varepsilon^{d+1} \cdot \dot{\varepsilon} \quad \text{Equation 8}$$

Summing up the two sides of equations 6 and 8, Equation (9) can be written as:

$$\frac{E_i(\varepsilon) + E_r(\varepsilon)}{2} = \frac{a}{b+1} \cdot \varepsilon^{b+1} \quad \text{Equation 9}$$

The energy input (E_i) and energy return (E_r) are equal to the areas below the stress-strain curve during loading and unloading respectively that were previously calculated through numerical integration (Equation 1 and 2). Parameters a and b can be calculated by fitting a power function to the average loading-unloading energy (that can also be referred to as elastic energy (E_e)) -strain data at strains from 0 to maximum strain (ε_{\max}).

Subtracting the two sides of equations 6 and 8, Equation (10) can be written as:

$$\frac{E_i(\varepsilon) - E_r(\varepsilon)}{2} = \frac{c}{d+1} \cdot \varepsilon^{d+1} \cdot \dot{\varepsilon} \quad \text{Equation 10}$$

The energy absorbed (E_h) during the entire loading cycle is the area between the loading and unloading in stress-strain curves, which was previously calculated by subtracting the areas below the curve during loading and unloading according to Equation (3). When the constant strain rate ($\dot{\epsilon}$) is known, parameters c and d can be calculated by fitting a power function to half of the absorbed energy-strain data at strains from 0 to maximum strain (ϵ_{\max}).

A bisquare curve fitting method was utilised that works by minimising the summed square of the residuals and downweight outliers (Matlab, Mathworks, 2010). Three fit goodness statistics were calculated including: the sum of squares due to error (SSE), where a value closer to zero indicating a fit that is more useful for prediction; R-square that is the square of the correlation between the response values and the predicted response values with a value closer to 1 indicating that a greater proportion of variance is accounted for by the model and RMSE that is the root mean squared error or standard error, with a value closer to 0 indicating a fit that is more useful for prediction (Curve Fitting Toolbox, Matlab, Mathworks, 2010) .

Statistical analyses

A series of statistical analyses was performed to provide insight into the physical meaning of the four parameters of the viscoelastic model used to describe the mechanical behaviour of the heel-pad. More specifically a paired wise sample T-test was utilised to assess the significance of the difference between the elastic and viscous model parameters to ensure that these two components are inherently different and that all these 4 model parameters (two scaling factors α and c and two exponents b and d) are required to address the mechanical behaviour of the heel pad effectively Pearson correlation analyses was used to investigate if the model parameters are influenced by the testing condition constants like target stress, strain rate, maximum strain. Furthermore Pearson correlation was used to investigate the relationship between the elastic model parameters and energy input per volume, energy return per volume, and between the viscous model parameters and energy absorbed per volume.

Results

As indicated in figure 3 the heel pad exhibits a strongly nonlinear mechanical behaviour during the indentation test. Initially the heel-pad appears to be very compliant, indeed relatively low stress (50kPa) are capable of generating significant strain (0.4). Moreover the difference between loading and unloading highlights the viscous nature of the heel-pad.

Figure 3 here

Figure 4 shows the elastic energy (E_e) and energy absorbed (E_h) and the power functions fitted to the data when the compression is performed at 0.057 s^{-1} strain rate and up to maximum strain of 0.45.

Figure 4 here

The results of the elastic and viscous stress-strain model parameters along with the fit goodness data are presented in Table 1, Table 2.

The comparison between the results for the test-retest that were performed at 0.051 s^{-1} up to max stress of 148 kPa and 0.052 s^{-1} up to max stress of 151 kPa revealed 1.0% variation in the elastic exponent (b) and 4.4 % variation in viscous exponent (d). This comparison also revealed 4.8 % variation in the elastic scaling factor (a) and 29.7 % variation in viscous scaling factor (c).

Table 1 here

Table 1 shows the elastic stress-strain reaction model parameters for the different maximum stress-strain rate conditions together with the fit goodness statistics.

Table 2 here

Table 2 shows the viscous stress-strain reaction model parameters for the different maximum stress-strain rate conditions together with the fit goodness statistics.

A significant correlation ($r=0.959$, $p = 0.003$) was found between the elastic exponent (b) and viscous exponent (d), while the paired sample T-test revealed a significant difference ($t=9.369$, $P=0.000$) between these two parameters ($b=3.965 \pm 0.709$ vs $d=2.117 \pm 0.492$).

While a significant difference ($t=14.032$, $P=0.000$) was found between the elastic scaling factor (a) ($1.348 \pm 0.337 \text{ MPa}$) and viscous scaling factor (c) ($0.096 \pm 0.036 \text{ MPa}$), no significant correlation was found between these two parameters ($p>0.01$).

Pearson correlation analysis revealed significant correlation ($r= 0.943$, $p= 0.005$) between the elastic exponent (b) and maximum strain. There was also significant correlation ($r= 0.936$, $p=0.006$) between the viscous exponent (d) and maximum strain.

Viscous scaling factor (c) was significantly ($r= 0.961$, $p=0.002$) correlated to maximum viscous stress (σ_v) and elastic scaling factor (a) was only significantly ($r= 0.834$, $p=0.039$) correlated to maximum elastic stress (σ_e).

Furthermore viscous scaling factor (c) was significantly correlated to viscous energy per volume (E_h) ($r= 0.905$, $p=0.013$).

Elastic energy per volume (E_e) – (12.853 ± 3.165 kPa) at maximum strain was significantly ($t=10.069$, $P=0.000$) higher than energy absorbed per volume (E_h) (3.953 ± 1.517 kPa) at maximum strain.

Maximum elastic stress (σ_e) (117.083 ± 27.122 kPa) was significantly ($t=10.069$, $P=0.000$) higher than maximum viscous stress (σ_v) (23.916 ± 8.825 kPa).

Discussion

The method proposed in this study showed to be able to differentiate between the viscous and elastic components of heel pad mechanical behaviour. In this approach the energy input and energy return were calculated first by numerical integration of the area below the stress strain curve up to the maximum strain during loading and unloading respectively. The average of the energy input and energy return as well as the energy absorbed as a result of Hysteresis was calculated by subtracting the energy return from the energy input at each strain.

Then the elastic and viscous energy functions were obtained by integration of a nonlinear visco-elastic model. To determine the corresponding scaling factor and exponent for the two components, the obtained elastic and viscous energy functions were fitted to the elastic energy-strain and hysteresis-strain data. The fit goodness statistics showed a high coefficient of determination and a low standard error of estimates (Table 1 and 2). Generally the method of quantifying the viscous and elastic scaling factor and exponent of heel pad showed to be able to provide a robust way of determining these parameters.

It was observed that the elastic energy (E_e) was significantly (3.2 fold) higher than the absorbed Energy (E_h), while the elastic stress (σ_e) was significantly higher than the viscous stress (σ_v). Furthermore such significant difference was also observed for the scaling factor (1.9 times higher for elastic) and exponent (14 times higher for viscous). This indicates that a higher proportion of reaction force to be from the elastic component, and a dominant role of elasticity (as compared to viscosity) in the tested condition for this particular heel pad.

Due to the manual operation of the indentation device, the achieved maximum interface pressure (stress) and loading rate was slightly different ($\pm 6.9\%$) than the nominal selected target strain rate. This has

been identified as the main source of error and in future studies a motorised loading apparatus need to be employed to control the variability in the deformation rate. This could have affected the results of test-retest that was intended to be performed at identical target stress and strain rate. While both the elastic and viscous exponents and elastic scaling factor showed low variations (less than 5%) between the two testing conditions, the viscous scaling factor showed much higher variations (29.7%) between the two tests. This in addition to the differences between the maximum stress that was achieved due to manual operation of the device could be attributed to the effect of loading history as a result of preloading. Generally the variations in the exponent were less than the variation in scaling factor, which may indicate that the exponent is more deterministic of the behaviour of plantar soft tissue during loading, hence may have implications in diagnosing the plantar soft tissue mechanical malfunction.

While the elastic or viscous scaling factors (a , c) do not seem to be dependent on maximum strain or the target stress, significant ($p < 0.01$) correlations between elastic scaling factor and maximum elastic stress and a significant correlation ($p < 0.05$) between viscous scaling factor and viscous stress were found in this study. These can indicate a more deterministic role of elastic and viscous scaling factors as two non-correlated parameters that are significantly different – (as compared to corresponding exponents that are significantly different and correlated) - in determining maximum elastic and viscous stress.

While the viscous and elastic exponents reveal the shape curvature of the stress strain graph, the existence of significant correlation between maximum strain and both the elastic and viscous exponents show that these two parameters are dependent on the maximum strain to which the soft tissue deforms due to a phenomenon known as strain stiffening. This was previously attributed to the nonlinear (curvilinear) stress-strain relationship inherent in biological visco-elastic structures where extrapolation of the mechanical properties can cause large errors [33]. This indicates that in using these parameters to quantify the behaviour of heel pad a certain target strain needs to be introduced and implicated to avoid inconsistency in the calculated parameters. Since the higher maximum strain the higher the exponents, for quantifying realistic parameters the soft tissue need to be deformed to the level over which it compressed during specific weight bearing activity i.e. walking and standing.

In fact both the viscous and elastic exponents of the reaction model parameter reveal the phenomenon known as strain stiffening that is a characteristic of visco-elastic biological soft tissue. In a sense since the strain stiffening depends on the amount of strain to which the tissue is subjected to, the exponents of stress strain curve can be identified as “strain stiffening indices”. These indices can determine the extent to which either elastic or viscous stiffness increase when strain increases. Although comparing the stress values at a set strain may also allow the comparison between the stiffness of different tissues, the comparison of exponents will determine the stress as a result of changes in curvature rather than the result of changes in scaling factor. Although both the value of stress at lower strains (determined mainly by the scaling factor) and the strain stiffening (determined by the exponent) affect the viscous and elastic stress and the interplay between the two. In fact the stress-strain relationship of a heel pad is determined by the cumulative mechanical responses of the different layers of adipose tissues and skin. Specifically the strain stiffening of the heel pad under compression loading has been attributed to the collagen fibres of the fat pad and skin becoming under tension at higher strains and resulting in an excess increase in stress hence an increase in the stiffness [28].

In most previous in-vivo studies [17] [13] [8] [19] the maximum load applied to the plantar soft tissue were much lower than the actual load applied to the heel pad during locomotion. In this study the maximum load was adjusted at three different levels corresponding to the maximum load during standing and walking barefoot in the lab that corresponds to average plantar pressure 200 kPa.

Measuring the maximum strain during weight bearing activities of daily living like walking and running requires incorporating the measurement unit i.e. fluoroscopy [10] within the ground surface that can be difficult to achieve. Since this is not always possible and requires specific considerations, in testing the mechanical properties of plantar soft tissue maximum stress measured with either the pressure mats or plates (for barefoot conditions) or with in-shoe measurement device (for shod conditions) need to be taken into consideration. Given that for each individual the maximum pressure is a nonlinearly proportionate to the maximum strain up to which the soft tissue deforms, the inclusion of maximum

pressure as the upper limit of stress up to which the soft tissue is tested ensures that the quantified elastic and viscous components are valid within the range that the soft tissue is loaded.

Since the viscous scaling factor (c) showed to be significantly correlated to both the maximum viscous stress and energy absorbed, it can be speculated that when higher viscous stress is reached, a change in the structure of plantar heel pad lead to a systematic increase in the energy absorbed. While this could be affected by the different pre-loading of the soft tissue, the observed correlation may be linked to the compression of the micro-structure of fat at higher applied stress that leads also to further compression of macro chambers.

To shed more light on the stress- strain model parameters and the effect of compression on each layer of heel pad, further studies are needed to be conducted with high resolution image modalities that can differentiate between the different layers of soft tissue. Such studies need to be backed up by histological observations to shed more light on the interconnection between the compression of micro and macro chambers and the role these play with regards to energy absorbed during loading.

It has been reported that the loading rate affects the stiffness of plantar soft tissue [15, 33, 34]. While the tests in this study were performed in a displacement control mode, no significant correlation was found between the strain rate and the stress-strain model parameters. This emphasises that for the viscous component that is a linear function of deformation rate, the damping force, hence the total stiffness increase with an increase in the deformation rate that is in line with the previous findings.

Furthermore due to the manual operation of the device, achieving a consistent strain rate was not feasible at a higher level (i.e. $> 7.4 \%s^{-1}$) and hence the results of this study cannot be extrapolated to higher strain rates.

There has been a scarcity of methods that can quantify the viscous and elastic component of stress and to quantify stress-strain model parameters for the heel pad. The method proposed here enables studies of the heel pad mechanical behaviour, which can be influenced by diseases such as diabetes, in light of these parameters. For example the heel pad tissue showed a diminished cushioning ability of diabetic heel region was reported by Hsu et al [13], while a linear stress/strain relationship that can be considered as an oversimplification of the soft tissue force deformation behaviour was assumed.

This study also reported an increase stiffness of macrochambers and a decreased stiffness of microchambers [13] as a result of diabetes. In future the method reported within this study can be applied to the different layers of soft tissue including the skin, micro and macro chambers of the fat pad to quantify the stress-strain behaviour of each layer.

When the viscous reaction parameters (c and d) and the strain rate are known, hysteresis can be calculated based on Equation 10. The energy absorbed and the elastic energy (reported in Table 1 and 2) can be used to calculate the energy-return efficiencies as the ratio of hysteresis to energy input. This is found to be between 72-81 % for the range of strain rates achievable in this study, and may vary during compressions at higher strain rates.

Considerations and limitations

It should be emphasised that, although the indentation provides realistic compressive forces to the plantar soft tissue, the effect of shear and the interaction between the loaded area (the probe to bone volume of interest) and the adjacent unloaded area cannot be modelled with the proposed method in this study. Furthermore specific attention need to be given to the maximum load applied to the heel due to the nature of loading during indentation in which only a volumetric strip of the heel pad is loaded , instead of the entire heel pad that is loaded during walking. During indentation with the probe in the frontal plane, an additional shear stress may develop between the loaded and unloaded tissue that does not exist at the same level during walking. This needs to be taken into consideration to ensure safety in terms of overloading the tissue and causing injury and for modeling purposes.

Furthermore while the parameters reported in this study are subject-specific, the parametric model used and the method proposed to find these parameters can be applied to any set of stress-strain data gathered during dynamic cyclic loading of the heel pad at constant deformation rate.

Although the procedure explained in this manuscript can be applied to quantify the foot-specific viscous and elastic reaction model parameters of heel pad, the effect of target stress and strain rate on the quantified reaction model parameters may be somehow different for a different participant than what is

found and reported in the current study. This can be due to differences in the mechanical properties of plantar soft tissue as a result of variations in material properties of the geometry of the heel pad between individuals. Even though the mechanical properties of plantar soft tissue can also be extracted from inverse Finite Element analysis [22], the method proposed in the present paper can independently identified the viscous and elastic parameters. Moreover a Finite Element Approach was beyond the scope of this study.

Implications in diagnosis

The proposed method of quantifying the heel pad mechanical behaviour can have huge implications in diagnosing the heel pad's mechanical viability and its vulnerability to trauma. While through the proposed method the elastic and viscous reaction model parameters can be identified and a threshold for each parameter can be set over which the soft tissue behaviour falls outside the healthy behaviour. These thresholds may be patient specific and can be identified through longitudinal assessments and upon development can have huge implications in diagnosis and identifying the risk of heel pad trauma in relation to a variety of pathologies. In future the method proposed in this study can be applied to quantify the viscosity and elasticity and strain stiffening of these two components for each of the constitutive layers of the plantar soft tissue, based on which a more detailed assessment of plantar soft tissue vulnerability to mechanical trauma may be attained.

Conclusion

The proposed method was able to differentiate between the elastic and viscous components of soft tissue response to loading and to quantify the corresponding stress-strain model parameters. Some of quantified model parameters showed to be correlated to the maximum stress. This method can have potential implications in quantifying the mechanical behaviour of the heel pad during compression, and in determining a detailed understanding of fat pad behaviour in realistic loading conditions.

References:

1. Bennett MB, Ker RF (1990) The mechanical properties of the human subcalcaneal fat pad in compression. *J Anat* 171:131–8.
2. Whittle MW (1999) Generation and attenuation of transient impulsive forces beneath the foot: a review. *Gait Posture* 10:264–75.
3. Jahss MH, Michelson JD, Desai P, et al. (1992) Investigations into the fat pads of the sole of the foot: anatomy and histology. *Foot Ankle* 13:233–42.
4. Jørgensen U, Bojsen-Møller F (1989) Shock absorbency of factors in the shoe/heel interaction--with special focus on role of the heel pad. *Foot Ankle* 9:294–9.
5. Aerts P, Ker RF, de Clercq D, Ilesley DW (1996) The effects of isolation on the mechanics of the human heel pad. *J Anat* 188 (Pt 2):417–23.
6. Aerts P, De Clercq D (1993) Deformation characteristics of the heel region of the shod foot during a simulated heel strike: the effect of varying midsole hardness. *J Sports Sci* 11:449–61. doi: 10.1080/02640419308730011
7. Aerts P, Ker RF, De Clercq D, et al. (1995) The mechanical properties of the human heel pad: a paradox resolved. *J Biomech* 28:1299–308.
8. Challis JH, Murdoch C, Winter SL (2008) Mechanical properties of the human heel pad: a comparison between populations. *J Appl Biomech* 24:377–81.
9. Gefen A (2003) Plantar soft tissue loading under the medial metatarsals in the standing diabetic foot. *Med Eng Phys* 25:491–499. doi: 10.1016/S1350-4533(03)00029-8
10. Gefen A, Megido-Ravid M, Itzchak Y (2001) In vivo biomechanical behavior of the human heel pad during the stance phase of gait. *J Biomech* 34:1661–5.
11. Gilchrist LA, Winter DA (1996) A two-part, viscoelastic foot model for use in gait simulations. *J Biomech* 29:795–8.
12. Gilchrist LA, Winter DA (1997) A multisegment computer simulation of normal human gait. *IEEE Trans Rehabil Eng* 5:290–9.
13. Hsu T, Lee Y, Shau Y (2002) Biomechanics of the heel pad for type 2 diabetic patients. *Clin Biomech* 17:291–296.
14. Miller RH, Hamill J (2009) Computer simulation of the effects of shoe cushioning on internal and external loading during running impacts. *Comput Methods Biomech Biomed Engin* 12:481–90. doi: 10.1080/10255840802695437
15. Ledoux WR, Blevins JJ (2007) The compressive material properties of the plantar soft tissue. *J Biomech* 40:2975–81. doi: 10.1016/j.jbiomech.2007.02.009
16. Miller-Young JE, Duncan NA, Baroud G (2002) Material properties of the human calcaneal fat pad in compression: experiment and theory. *J Biomech* 35:1523–31.

17. Chao CYL, Zheng Y-P, Huang Y-P, Cheing GL-Y (2010) Biomechanical properties of the forefoot plantar soft tissue as measured by an optical coherence tomography-based air-jet indentation system and tissue ultrasound palpation system. *Clin Biomech (Bristol, Avon)* 25:594–600. doi: 10.1016/j.clinbiomech.2010.03.008
18. Cole GK, Nigg BM, van Den Bogert AJ, Gerritsen KGM (1996) The clinical biomechanics award paper 1995 Lower extremity joint loading during impact in running. *Clin Biomech (Bristol, Avon)* 11:181–193.
19. Rome K, Webb P, Unsworth A, Haslock I (2001) Heel pad stiffness in runners with plantar heel pain. *Clin Biomech (Bristol, Avon)* 16:901–5.
20. Zheng YP, Choi YK, Wong K, et al. (2000) Biomechanical assessment of plantar foot tissue in diabetic patients using an ultrasound indentation system. *Ultrasound Med Biol* 26:451–6.
21. Wearing SC, Smeathers JE, Yates B, et al. (2009) Bulk compressive properties of the heel fat pad during walking: a pilot investigation in plantar heel pain. *Clin Biomech (Bristol, Avon)* 24:397–402. doi: 10.1016/j.clinbiomech.2009.01.002
22. Erdemir A, Viveiros ML, Ulbrecht JS, Cavanagh PR (2006) An inverse finite-element model of heel-pad indentation. *J Biomech* 39:1279–86. doi: 10.1016/j.jbiomech.2005.03.007
23. Hsu TC, Wang CL, Shau YW, et al. (2000) Altered heel-pad mechanical properties in patients with Type 2 diabetes mellitus. *Diabet Med* 17:854–9.
24. Hsu C-C, Tsai W-C, Shau Y-W, et al. (2007) Altered energy dissipation ratio of the plantar soft tissues under the metatarsal heads in patients with type 2 diabetes mellitus: a pilot study. *Clin Biomech (Bristol, Avon)* 22:67–73. doi: 10.1016/j.clinbiomech.2006.06.009
25. Tong J, Lim C., Goh O. (2003) Technique to study the biomechanical properties of the human calcaneal heel pad. *Foot* 13:83–91. doi: 10.1016/S0958-2592(02)00149-9
26. Hsu C-C, Tsai W-C, Hsiao T-Y, et al. (2009) Diabetic effects on microchambers and macrochambers tissue properties in human heel pads. *Clin Biomech (Bristol, Avon)* 24:682–6. doi: 10.1016/j.clinbiomech.2009.06.005
27. Natali N, Fontanella CG, Carniel EL, Young JM (2011) Biomechanical behaviour of heel pad tissue experimental testing, constitutive formulation, and numerical modelling. *Proc Inst Mech Eng Part H J Eng Med* 225:449–459. doi: 10.1177/09544119JEIM851
28. Natali N, Fontanella CG, Carniel EL (2010) Constitutive formulation and analysis of heel pad tissues mechanics. *Med Eng Phys* 32:516–22. doi: 10.1016/j.medengphy.2010.02.018
29. Gerritsen KG, van den Bogert AJ, Nigg BM (1995) Direct dynamics simulation of the impact phase in heel-toe running. *J Biomech* 28:661–8.
30. Scott SH, Winter DA (1993) Biomechanical model of the human foot: kinematics and kinetics during the stance phase of walking. *J Biomech* 26:1091–1104.
31. Naemi R, Chockalingam N (2013) Mathematical models to assess foot-ground interaction: an overview. *Med Sci Sports Exerc* 45:1524–33. doi: 10.1249/MSS.0b013e31828be3a7

32. Chatzistergos PE, Naemi R, Sundar L, et al. (2014) The relationship between the mechanical properties of heel-pad and common clinical measures associated with foot ulcers in patients with diabetes. J Diabetes Complications (in–press).
33. Pai S, Ledoux WR (2010) The effect of target strain error on plantar tissue stress. J Biomech Eng 132:071001. doi: 10.1115/1.4001398
34. Pai S, Ledoux WR (2011) The quasi-linear viscoelastic properties of diabetic and non-diabetic plantar soft tissue. Ann Biomed Eng 39:1517–27. doi: 10.1007/s10439-011-0263-z

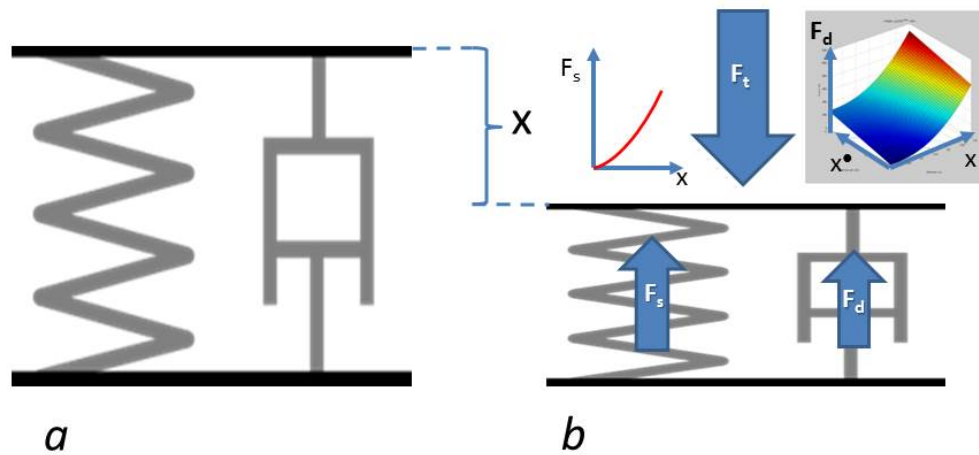


Figure 1: Nonlinear spring-damper model resembling the nonlinear visco-elastic behaviour of the heel pad under compression. Section *a* (on left) represents the uncompressed and section *b* (on right) represents the model under compression. x represent the deformation and \dot{x} represents the deformation rate. F_t is the total compression force and F_s and F_d represent the reaction forces by spring and damper respectively. The following equations govern the mechanical behaviour of the system: $F_t = F_s + F_d$, $F_s = A \cdot x^B$, $F_d = C \cdot \dot{x}^D$. in which A and B are the elastic scaling factor and exponent reaction model parameters and C and D are the viscous scaling factor and exponent reaction model parameters respectively.

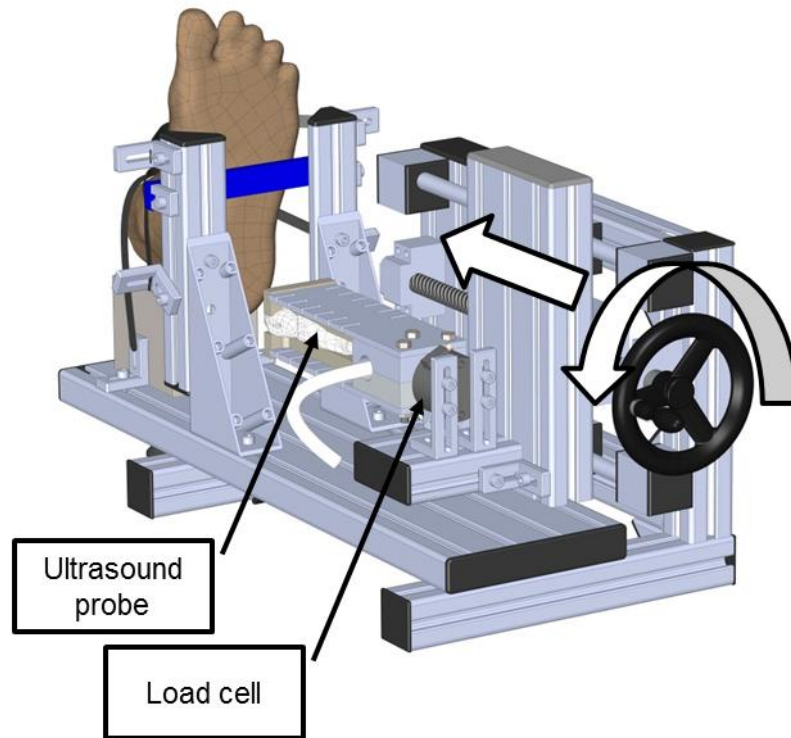


Figure 2: The ultrasound indentation device that was used for in-vivo mechanical testing of the heel pad.

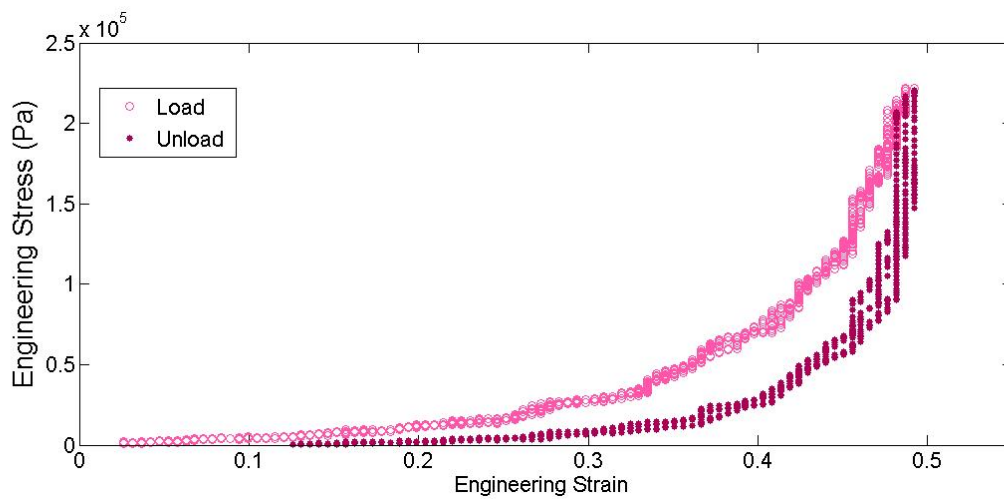


Figure 3: Representative stress-strain curve of the heel pad extracted using ultrasound indentation. The indentation test was performed at strain rate of 0.043 s^{-1} and at 210kPa maximum target stress.

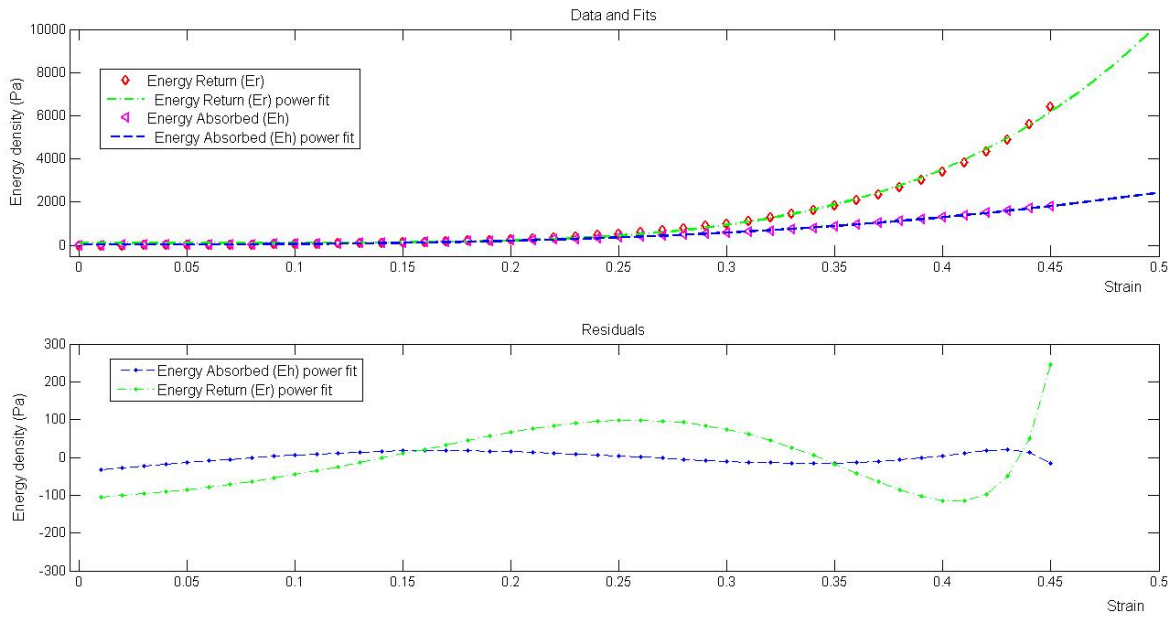


Figure 4. Representative results Elastic energy per volume (E_e) and Energy absorbed per volume (E_h) and the curve represented by Equations 8 and 9 fitted to the Energy-strain data (top), the residuals showing the difference between the actual value and the value predicted by the curve (bottom).

Maximum Stress (kPa)	Strain Rate	Maximum Strain	a (MPa)	b	SSE (10 ⁶)	R ²	RMSE	Elastic Energy density (kPa)	Maximum Elastic stress (kPa)
148.4	0.052 ± 0.003	0.476	1.480	3.514	3.149	0.992	264.5	11.490	108.964
151.7	0.051 ± 0.002	0.492	1.382	3.463	5.4	0.991	339.0	13.063	118.496
144.5	0.044 ± 0.003	0.613	1.438	5.056	2.539	0.995	207.5	12.261	121.129
158.1	0.073 ± 0.005	0.513	1.784	3.742	6.369	0.992	360.5	15.882	146.810
70.4	0.057 ± 0.004	0.45	0.761	2.997	0.9897	0.995	151.7	7.822	69.479
201.9	0.043 ± 0.003	0.524	1.245	3.401	5.303	0.993	329.0	16.459	138.239

Table 1. The elastic stress-strain model parameters for the different target strain- strain rate conditions along with the fit goodness statistics.

Maximum Stress (kPa)	Strain Rate	Maximum Strain	c (MPa)	d	SSE (10 ⁶)	R ²	RMSE	Energy absorbed density (kPa)	Maximum Viscous stress (kPa)
148.4	0.052 ± 0.003	0.476	0.090	1.931	0.173	0.996	61.9	3.491	21.494
151.7	0.051 ± 0.002	0.492	0.138	2.056	0.337	0.997	84.7	5.171	32.120
144.5	0.044 ± 0.003	0.613	0.106	3.091	0.080	0.999	36.9	3.490	23.290
158.1	0.073 ± 0.005	0.513	0.072	1.889	0.149	0.997	55.2	3.629	20.436
70.4	0.057 ± 0.004	0.45	0.042	1.715	0.026	0.998	24.6	1.791	10.803
201.9	0.043 ± 0.003	0.524	0.130	2.017	0.441	0.997	94.9	6.149	35.404

Table 2. The viscous stress-strain model parameters for the different target strain- strain rate conditions along with the fit goodness statistics.